AGU PUBLICATIONS

Water Resources Research

TECHNICAL REPORTS: DATA

10.1002/2014WR016559

Key Points:
- We discuss scaling of the hyporheic BTCs simulated by our Lagrangian model
- The skewness of the BTC is constant over a wide range of streambed morphologies
- Scaling of the first three BTC moments is consistent with experimental data

Correspondence to:
A. Bellin,
alberto.bellin@ing.unitn.it

Citation:
Bellin, A., D. Tonina, and A. Marzadri (2015), Breakthrough curve moments scaling in hyporheic exchange, *Water Resour. Res.*, *51*, 1353–1358, doi:10.1002/2014WR016559.

Received 14 OCT 2014
Accepted 6 JAN 2015
Accepted article online 14 JAN 2015
Published online 11 FEB 2015

Breakthrough curve moments scaling in hyporheic exchange

A. Bellin[1], D. Tonina[2], and A. Marzadri[2]

[1]Department of Civil, Environmental and Mechanical Engineering, University of Trento, Trento, Italy, [2]Center for Ecohydraulics Research, University of Idaho, Boise, Idaho, USA

Abstract The interaction between stream flow and bed forms creates an uneven distribution of near-bed energy heads, which is the driving force of hyporheic exchange. Owing to the large disparity of advection characteristic times in the stream and within the hyporheic zone, solute mass exchange is often modeled by considering the latter as an immobile region. In a recent contribution Gónzalez-Pinzón et al. (2013) showed that existing models employing this hypothesis are structurally inconsistent with the scaling revealed by the analysis of 384 breakthrough curves collected in 44 streams across five continents. Motivated by this result, we analyze the scaling characteristics of a model that we recently developed by combining the analytical solution of the advective flow within the hyporheic zone with a Lagrangian solute transport model. Results show that similarly to the experimental data our model predicts breakthrough curves with a constant skewness, irrespective of the stream size, and that the scaling of the first three moments observed by Gónzalez-Pinzón et al. (2013) is also respected. Moreover, we propose regression curves that relate the first three moments of the residence time distribution with the alternate bar dimensionless depth (Y^*_{BM}), a quantity that is easily measurable in the field. The connection between BTC moments and Y^*_{BM} opens new possibilities for modeling transport processes at the catchment scale.

1. Introduction

The hyporheic zone, typically identified as the saturated sediment volume beneath and around a stream, is a biologically sensitive zone sustaining and nurturing the benthic population, which is an important component of the food chain in freshwater ecosystems [*Stanford and Ward*, 1993; *Battin et al*., 2008; *Gooseff*, 2010], and of crucial importance in the first stages of the salmonids life cycle [*Tonina and Buffington*, 2009a; *Gariglio et al*., 2013]. The hyporheic zone (HZ) is also an important ecotone, where hot spots of geochemical processes play a relevant role in nutrients cycling and contaminant transformations [*Briggs et al*., 2013; *Harvey et al*., 2013]. The biological activity in the HZ is chiefly controlled by forces driving water into the surrounding sediments [*Edwards*, 1998]. The most relevant driving force is generated by the uneven distribution of near-bed energy heads (pumping process), which create downwelling fluxes in high energy areas combined with upwelling fluxes in low energy areas [*Tonina and Buffington*, 2009b]. Other mechanisms may contribute to the exchange, depending on stream morphology, such as turbulence in the stream current and suspended sediment transport, which may lead to the emergence of density driven exchanges between stream and pore waters [see *Tonina*, 2012, and references therein]. Within the hyporheic zone, the development of ecological niches is favored by less extreme environmental conditions with respect to the stream: flow is much slower and less variable than in the stream, while dial and seasonal changes of water temperature are significantly damped [*Marzadri et al*., 2013a, 2013b]. Tracer tests evidenced that stream water entering the hyporheic zone through downwelling areas resides within the sediments much longer than the water traveling similar distances in the stream [*Haggerty et al*., 2002]. This observation suggested the use of mobile-immobile schemes for modeling exchanges between the stream and surrounding sediments [see e.g., *Boano et al*., 2014, for a review].

In a recent contribution, *Gónzalez-Pinzón et al*. [2013] analyzed 384 Breakthrough Curves (BTCs) of nonreactive tracers recorded in 44 stream reaches of length ranging from 10 m to 10 km, with water discharge spanning 6 log-scales from $10^{-3} m^3/s$ to $10^3\ m^3/s$. The wide range of scales covered by the data provide a valid benchmark for testing the performance of several available transport models.

These data are important because the BTC of a nonreactive tracer recorded downstream an injection point bears the signature of the exchange with the hyporheic zone, in addition to mixing in the stream water. Where the signature of hyporheic exchange is more evident is in the tail of the BTC, which decays more slowly than expected if the transport was purely diffusive [see e.g., *Haggerty et al*., 2002]. A relatively simple way to assess the relevance of hyporheic exchange, and its evolution downstream the injection points, is through the third centered temporal moment of the BTC, or its dimensionless counterpart, the skewness coefficient (CSK), because both are asymmetry measures sensitive to the extension of the tailing in the BTC.

The most striking outcome of the analysis conducted by *Gónzalez-Pinzón et al*. [2013] is that most of the widely used models of hyporheic exchange are not consistent with the scaling of the skewness coefficient emerging from the BTCs analysis. A first model not consistent with this observed scaling is the widely used Transient Storage Model (TSM) [*Bencala and Walters*, 1983], which is based on the solution of the advection-dispersion equation in the stream with the hyporheic zone modeled as an immobile zone exchanging solute mass with the stream through a diffusive exchange term. Successively to its introduction, generalizations of TSM, such as the Aggregated Dead Zone Model (ADZM) and multiple exchange rates, have been proposed with the aim to improve the description of the advective exchange, which is not adequately reproduced by TSM [*Haggerty and Gorelick*, 1995]. In another attempt to better quantify hyporheic exchange, *Boano et al*. [2007] used the decoupled Continuous Time Random Walk (dCTRW) theory to model the transient storage effect in terms of a waiting time probability density function. Also these, more sophisticated models, are inconsistent with the scaling between the BTC moments emerging from the 384 BTCs. None of these models, in fact, is able to reproduce the observed scaling between the temporal moments of the experimental BTCs, unless a fitting is performed by letting model parameters to vary with the distance, in clear violation of the assumptions at the base of their theoretical derivation [*Gónzalez-Pinzón et al*., 2013].

In the present work, we show that an alternative modeling approach, which we developed recently [*Marzadri et al*., 2010] to analyze hyporheic BTCs, reproduces the same scaling unveiled by *Gónzalez-Pinzón et al*. [2013] without violating the base assumptions underlying its development.

2. Material and Methods

In our approach, exchange with the hyporheic zone is modeled within a Lagrangian framework, through the residence time theory, which allows taking into account the diversity of flow pathways that characterize the hyporheic exchange. In the hyporheic zone, residence time can be defined as the time that a particle of tracer, transported without reaction, spends within the alluvium while it travels from downwelling to upwelling surfaces. Within this framework and assuming, in first approximation, that flow is at steady state, an equivalence can be established between the statistical moments of the residence time τ and the BTC moments [*Dagan et al*., 1992; *Bellin and Rubin*, 2004]. When flow is nonstationary a dynamic rescaling of time, expressed as the number of pore volumes crossing the upwelling surface up to the given time, allows using the solutions obtained for the stationary flow field [see e.g., *Zuber*, 1986; *Rinaldo et al*., 2011; *Ali et al*., 2014].

Following the analysis performed by *Gónzalez-Pinzón et al*. [2013], we consider the first three BTC centered moments:

$$\begin{aligned} m_1 &= \frac{1}{m_0}\int_0^\infty tC(t)dt \\ m_2 &= \frac{1}{m_0}\int_0^\infty (t-m_1)^2 C(t)dt \\ m_3 &= \frac{1}{m_0}\int_0^\infty (t-m_1)^3 C(t)dt \end{aligned} \tag{1}$$

where m_1 is the mean (or the first raw moment), m_2 and m_3 are the second and third centered moments, respectively. In addition, $C(t)$ is the flux concentration recorded over time at a fixed position and $m_0 = \int_0^\infty C(t)\,dt$ is the normalization constant.

The Skewness coefficient is defined as follows:

$$CSK = m_3/m_2^{3/2} \tag{2}$$

and is an indicator of tailing in the BTC [see e.g., *Das et al*., 2002; *Nauman and Buffham*, 1983].

Our hyporheic transport model is applied according to the following main steps [*Marzadri et al*., 2010]: (1) the spatial distribution of the hydraulic head at the streamed is obtained as a function of the water discharge Q, the stream water depth Y_0, and the channel width W, by using a standard hydrodynamic model [e.g., *Marzadri et al*., 2014a; *Tonina and Buffington*, 2009a; *Trauth et al*., 2013]. Stream-bed topography is needed at this stage, which can be measured [e.g., *McKean et al*., 2009], or inferred from available hydro-geomorphological models [e.g., *Colombini et al*., 1987; *Marzadri et al*., 2014b]; (2) the saturated Darcian flow within the alluvium is solved analytically with the hydraulic head at the streambed interface, provided by the hydrodynamic model, as boundary condition (see *Marzadri et al*. [2010] for a detailed discussion of the other boundary conditions and the geometry of the computational domain); (3) the residence time distribution is approximated by releasing a large number of particles within the downwelling region and marking the time they cross the upwelling region. Particle tracking is applied at this step of the procedure with the analytical flow field obtained at step 2 [e.g., *Tonina and Bellin*, 2008]. Notice that theories exist providing approximate analytical expressions of the distributions of the head at the streambed interface as a function of a few global hydrodynamic and morphological parameters, thereby avoiding the detailed characterization of the stream bed topography [*Elliott and Brooks*, 1997a; *Colombini et al*., 1987; *Stonedahl et al*., 2010; *Marzadri et al*., 2014a]. This procedure has been applied with success to a variety of morphologies described by means of a few general geomorphological characteristics [*Marzadri et al*., 2014b], thereby opening perspectives for upscaling geochemical processes from the reach to the network scale.

The travel time moments, evaluated by particle tracking, assume the following expressions:

$$m_1 = \frac{1}{NP}\sum_{i=0}^{i=NP}\tau_i$$
$$m_2 = \frac{1}{NP-1}\sum_{i=0}^{i=NP}(\tau_i - m_1)^2 \quad (3)$$
$$m_3 = \frac{1}{(NP-1)(NP-2)}\sum_{i=0}^{i=NP}(\tau_i - m_1)^3$$

where τ_i is the travel time of the i-th particle from the downwelling surface, where it is released, to the upwelling surface, where it is captured, and NP is the total number of particles released within the downwelling surfaces. In the following, we confront the scaling of these moments with that obtained from the experimental BTCs. Here we shall specify that our theoretical model provides the BTC of the hyporheic zone alone, while the experimental BTC includes also the effect of the solute traveling within the stream. However, owing to the large disparity between the residence times in the two compartments, we hypothesize that the scaling of the second and third BTC moments approaches that of the hyporheic BTC alone. This is in line with the approach used by *Gónzalez-Pinzón et al*. [2013], who analyzed the late time behavior of the model BTC moments in the absence of in stream dispersion to unveil the effect of temporary storage zones.

Our analysis is performed at the reach scale considering several morphological units spanning a rather wide range of channel's lengths ($L = 10 \div 188$m), width ($W = 1.5 \div 30$m), slopes ($s_0 = 0.13 \div 2.64\%$), and discharges ($Q_S = 0.07 \div 51.9 m^3/s$) (see parameters reported in *Marzadri et al*. [2012, Table 1]). This is sufficient to assess to what extent our model reproduces the scaling revealed through the analysis of the BTCs, although the investigated range of hydro-morphological characteristics is somewhat narrower with respect to the cases investigated by *Gónzalez-Pinzón et al*. [2013].

3. Discussion

Figure 1 shows how the dimensionless first normalized moment, $m_1^* = m_1/t_f$, and the following two normalized central moments $m_2^* = m_2/(t_f)^2$ and $m_3^* = m_3/(t_f)^3$ scale with respect to the dimensionless stream depth $Y_{BM}^* = Y_0/H_{BM}$. Here H_{BM} is the bed form amplitude for alternate bars, which we obtained from the empirical relationship proposed by *Colombini et al*. [1987]. Similar expressions, either based on hydro-morphological theories or empirical relationships, are available for pool and riffle and dune bed forms [*Marzadri et al*., 2014b]. As reported by *Marzadri et al*. [2010] $t_f = L/(K_h s_0 C_z)$ is a suitable advective characteristics time scale, where L is the bed form length, K_h is the streambed material hydraulic conductivity, s_0 is the streambed slope, C_z is the dimensionless Chezy coefficient and Y_{BM}^* is a function of the morphodynamic parameters

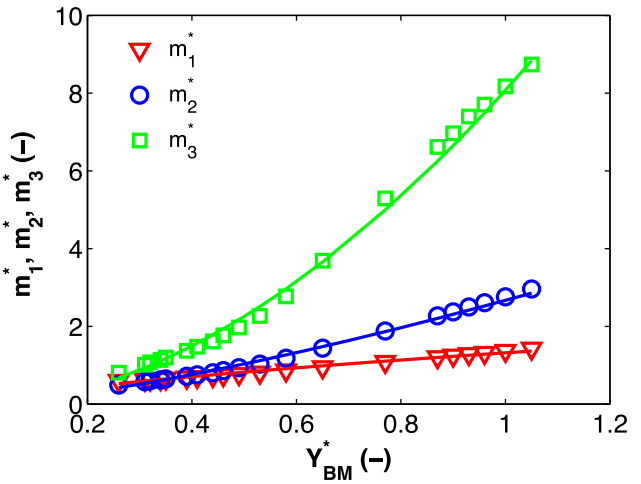

Figure 1. Dimensionless first (open red triangles), second (open blue circles) and third (open green squares) temporal moments of the hyporheic residence time distributions as a function of the alternate bar dimensionless depth ($Y^*_{BM}=Y_0/H_{BM}$) for 20 different morphologies developing alternate bars [see *Marzadri et al.*, 2012, Table 1]. The following regression equations are also shown (determination coefficient within brackets): $m^*_1=1.32Y^{*\,0.67}_{BM}$ (red curve, $R^2=0.98$); $m^*_2=2.67Y^{*\,1.37}_{BM}$ (blue curve, $R^2=0.99$); $m^*_3=8.08Y^{*\,1.84}_{BM}$ (green curve, $R^2=0.99$).

controlling the near-bed pressure distribution (and the hyporheic exchange through it; see *Marzadri et al.* [2012, equation (15)]). The first three residence time moments scale with Y^*_{BM}, according to the following power law functions:

$$m^*_1=1.32(Y^*_{BM})^{0.68}R^2=0.98,$$
$$m^*_2=2.67(Y^*_{BM})^{1.37}R^2=0.99, \quad (4)$$
$$m^*_3=8.08(Y^*_{BM})^{1.84}R^2=0.99,$$

which are obtained by regression of the power law expression: $m^*_i=a_iY^{*\,\beta_i}_{BM}$, $i=1, 2, 3$ to the estimates of the theoretical moments obtained by means of the equations (3). Notice that the rather high coefficient of determination R^2 indicates that most of the variability in the moments predicted by our model is explained by the equations (4).

Figure 2 shows with open circles the third dimensionless moment m^*_3 versus the second dimensionless moment m^*_2 predicted by our model with reference to the range of cases reported in *Marzadri et al.* [2012, Table 1]. In addition, the following expression of the third centered moment can be obtained, under the hypothesis that the skewness *CSK* is constant, as suggested by *Gónzalez-Pinzón et al.* [2013] (equation (7)) on the basis of the experimental BTCs:

$$m^*_3=CSK\,m^{*\,1.5}_2 \quad (5)$$

This expression, evaluated with $CSK=2.12$, which is the mean skewness coefficient obtained from the theoretical moments provided by our model, is depicted with the black dashed curve in Figure 2. The determination coefficient R^2 of this curve (without fitting) is 0.96, indicating that 96% of the variation is explained by the expression (5). On the other hand, the expression $m^*_3=2.16\,(m^*_2)^{1.34}$, obtained by combining the second with the third equation of (4) shows a determination coefficient of $R^2=0.99$ (red curve in Figure 2). Notice that *Gónzalez-Pinzón et al.* [2013] obtained a similar determination coefficient ($R^2=0.98$) by applying the expression (5) to the experimental BTCs.

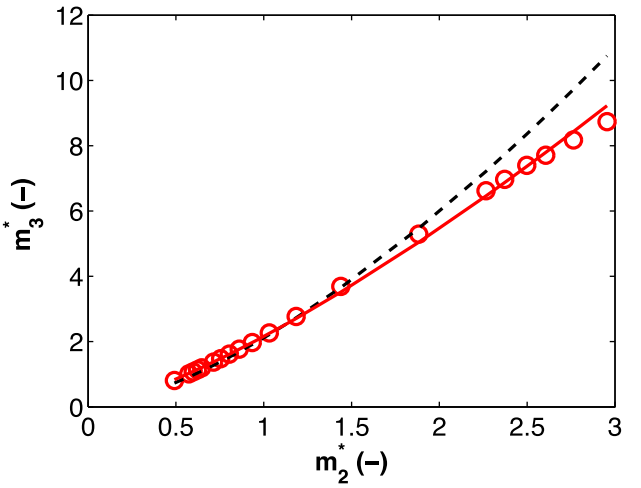

Figure 2. Relations between the dimensionless third and second temporal moments for 20 different stream morphologies developing alternate bars [see *Marzadri et al.*, 2012, Table 1]. The following scaling models are also shown (determination coefficient within brackets): $m^*_3=2.16\,m^{*\,1.34}_2$ (red curve, $R^2=0.99$); $m^*_3=2.12\,m^{*\,1.5}_2$ (black dashed curve, $R^2=0.96$).

The observation that for the experimental BTCs both the coefficient of variation and the skewness are roughly constant suggested to *Gónzalez-Pinzón et al.* [2013] the following linear scaling of m_3 with the product m_1m_2:

$$m_3=CSK\,CVm_1m_2 \quad (6)$$

Figure 3 shows the comparison of this scaling (red line) with the theoretical moments of our model (open red symbols). Equation (6) is shown in

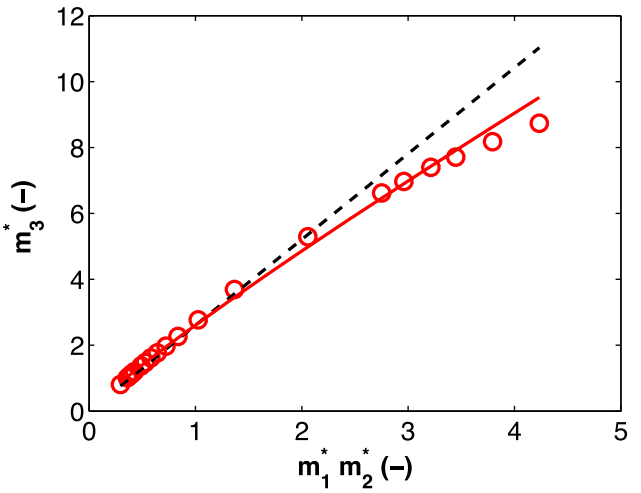

Figure 3. Relations between the third dimensionless moment m_3^* and the dimensionless factor $(m_1^* m_2^*)$ for 20 different stream morphologies developing alternate bars [see *Marzadri et al.*, 2012, Table 1]. The following scaling models are also shown (determination coefficient within brackets): $m_3^* = 2.608(m_1^* m_2^*)$ (black dashed curve, $R^2 = 0.96$); $m_3^* = 2.608(m_1^* m_2^*)^{0.89}$ (red curve, $R^2 = 0.99$).

Figure 3 (black dashed line) with the product *CSK CV* set to 2.608, which is the value obtained by multiplying the mean value of $CSK = 2.12(0.20)$ by the mean value of $CV = 1.23(0.02)$, where the number within brackets indicates the standard deviation. The determination coefficient in this case is $R^2 = 0.96$.

Another way to express this scaling is by substituting into the third equation of (4) the expression of Y_{BM}^* obtained from inversion of the product of the first two equations, which leads to: $ln(m_3^*) = 0.897 ln(m_1^* m_2^*) + ln(2.608)$. This scaling is depicted in Figure 3 with the red line and results in a determination coefficient of $R^2 = 0.99$. Furthermore, the scaling exponent of 0.897 compares well with the experimental value of $\gamma = 0.932$ that *Gónzalez-Pinzón et al.* [2013] obtained by regression of the relationship $ln(m_3) = \gamma\, ln(m_1 m_2)$ ($R^2 = 0.96$) to the BTCs moments of the experimental data set [see *Gónzalez-Pinzón et al.*, 2013, Figure 2].

4. Summary and Conclusions

We showed that our modeling approach, differently from most of the existing and widely used reach-scale transport models, reproduces very closely the scaling of the first three temporal moments unveiled by *Gónzalez-Pinzón et al.* [2013] with the analysis of a large data set of experimental BTCs, spanning a wide range of hydro-morphological characteristics.

We also showed that the first three normalized temporal moments are well represented by three power law relationships, which connect the residence time distribution directly to stream morphology, through the dimensionless depth $Y_{BM}^* = Y_0 / H_{BM}$, a quantity that can be easily obtained from field data.

These evidences let us to conclude that our model is consistent with the scaling among the first three BTC moments unveiled by *Gónzalez-Pinzón et al.* [2013] from the analysis of a large BTCs data set. In addition, it is easy to apply and requires rather standard measurable quantities, thereby minimizing the need of expensive, time consuming, and hardly generalizable local reach-scale field experiments. On the other hand, this equivalent in scaling behavior suggests that the hypothesis of transport processes dominated by river morphology, which we introduced in previous publications, is actually consistent with the available data.

Acknowledgments
All the data used in this work are included in Table 1 of a referenced paper [*Marzadri et al.*, 2012]. The first author acknowledges the funding of the European Communities 7th Framework Programme, under grant agreement 603629-ENV-2013-6.2.1-Globaqua, and of the Italian Ministry of Public Instruction, University and Research through the project PRIN 2010–2011, protocol 2010JHF437: Innovative methods for water resources management under hydroclimatic uncertainty scenarios.

References

Ali, M., A. Fiori, and D. Russo (2014), A comparison of travel-time based catchment transport models, with application to numerical experiments, *J. Hydrol.*, *511*, 605–618, doi:10.1016/j.jhydrol.2014.02.010.

Battin, T. J., L. A. Kaplan, S. Findlay, C. S. Hopkinson, E. Marti, A. I. Packman, J. D. Newbold, and F. Sabater (2008), Biophysical controls on organic carbon fluxes in fluvial networks, *Nat. Geosci.*, *1*, 95–100, doi:10.1038/ngeo101.

Bellin, A., and Y. Rubin (2004), On the use of peak concentration arrival times for the influence of hydrogeological parameters, *Water Resour. Res.*, *40*, W07401, doi:10.1029/2003WR002179.

Bencala, K. E., and R. A. Walters (1983), Simulation of solute transport in a mountain pool-and-riffle stream: A transient storage model, *Water Resour. Res.*, *19*, 718–724.

Boano, F., R. Revelli, and L. Ridolfi (2007), Bedform induced hyporheic exchange with unsteady flows, *Adv. Water Resour.*, *30*(1), 148–156.

Boano, F., J. W. Harvey, A. Marion, A. I. Packman, R. Revelli, L. Ridolfi, and A. Wrman (2014), Hyporheic flow and transport processes: Mechanisms, models, and biogeochemical implications, *Rev. Geophys.*, *52*, doi:10.1002/2012RG000417, in press.

Briggs, M., L. Lautz, and D. Hare (2013), Residence time control on hot moments on net nitrate and uptake in hyporheic zone, *Hydrol. Processes*, *28*(11), 3741–3751.

Colombini, M., G. Seminara, and M. Tubino (1987), Finite-amplitude alternate bars, *J. Fluid Mech.*, *181*, 213–232.

Dagan, G., V. Cvetkovic, and A. M. Shapiro (1992), A solute flux approach to transport in heterogeneous formations: 1. The general framework, *Water Resour. Res.*, *28*, 1369–1376.

Das, B. S., R. S. Govindaraju, G. J. Kluitenberg, A. J. Valocchi, and J. M. Wraith (2002), Theory and applications of time moment analysis to study the fate of reactive solutes in soil, Stochastic Methods in Subsurface Contaminant Hydrology, pp. 239–279, doi:10.1061/9780784405321.ch06.

Edwards, R. T. (1998), The hyporheic zone, in *River Ecology and Management: Lessons From the Pacific Coastal Ecoregion*, edited by R. J. Naiman and R. E. Bilby, pp. 399–429, Springer, N. Y.

Elliott, A. H., and N. H. Brooks (1997a), Transfer of nonsorbing solutes to a streambed with bedforms: Theory, *Water Resour. Res.*, *33*, 123–136.

Gariglio, F., D. Tonina, and C. H. Luce (2013), Spatiotemporal variability of hyporheic exchange through a pool-riffle-pool sequence, *Water Resour. Res*, *49*, 7185–7204, doi:10.1002/wrcr.20419.

Gónzalez-Pinzón, R., R. Haggerty, and M. Dentz (2013), Scaling and predicting solute transport processes in streams, *Water Resour. Res.*, *49*, 4071–4088, doi:10.1002/wrcr.20280.

Gooseff, M. N. (2010), Defining hyporheic zones advancing our conceptual and operational definitions of where stream water and groundwater meet, *Geogr. Compass*, *4*(8), 945–955.

Haggerty, R., and S. M. Gorelick (1995), Multiple-rate mass transfer for modeling diffusion and surface reactions in media with pore-scale heterogeneity, *Water Resour. Res.*, *31*, 2383–2400.

Haggerty, R., S. M. Wondzell, and M. A. Johnson (2002), Power-law residence time distribution in the hyporheic zone of a 2nd-order mountain stream, *Geophys. Res. Lett.*, *29*(13), 1640, doi:10.1029/2002GL014743.

Harvey, J., J. Böhlke, A. M. Voytek, D. Scott, and C. Tobias (2013), Hyporheic zone denitrification: Controls on effective reaction depth and contribution to whole-stream mass balance, *Water Resour. Res.*, *49*, 6298–6316, doi:10.1002/wrcr.20492.

Marzadri, A., D. Tonina, A. Bellin, G. Vignoli, and M. Tubino (2010), Semi-analytical analysis of hyporheic flow induced by alternate bars, *Water Resour. Res.*, *46*, W07531, doi:10.1029/2009WR008285.

Marzadri, A., D. Tonina, and A. Bellin (2012), Morphodynamic controls on redox conditions and on nitrogen dynamics within the hyporheic zone: Application to gravel bed rivers with alternate-bar morphology, *J. Geophys. Res.*, *117*, G00N10, doi:10.1029/2012JG001966.

Marzadri, A., D. Tonina, and A. Bellin (2013a), Effects of stream morphodynamics on hyporheic zone thermal regime, *Water Resour. Res.*, *49*, 2287–2302, doi:10.1002/wrcr.20199.

Marzadri, A., D. Tonina, and A. Bellin (2013b), Quantifying the importance of daily stream water temperature fluctuations on the hyporheic thermal regime: Implication for dissolved oxygen dynamics, *J. Hydrol.*, *507*, 241–248.

Marzadri, A., D. Tonina, J. A. McKean, M. G. Tiedermann, and R. M. Benjankar (2014a), Multi-scale streambed topographic and discharge effects on hyporheic exchange at the stream network scale in confined streams, *J. Hydrol.*, *507*, 241–248, doi:10.1016/j.jhydrol.2013.10.030.

Marzadri, A., D. Tonina, A. Bellin, and J. L. Tank (2014b), A hydrologic model demonstrates nitrous oxide emissions depend on streambed morphology, *Geophys. Res. Lett.*, *41*, 5484–5491, doi:10.1002/2014GL060732.

McKean, J. A., D. Nagel, D. Tonina, P. Bailey, C. W. Wright, C. Bohn, and A. Nayegandhi (2009), Remote sensing of channels and riparian zones with a narrow-beam aquatic-terrestrial lidar, *Remote Sens.*, *1*, 1065–1096.

Nauman, E. B., and B. A. Buffham (1983), *Mixing in Continuous Flow Systems*, John Wiley, N. Y.

Rinaldo, A., K. J. Beven, E. Bertuzzo, L. Nicotina, J. Davies, A. Fiori, D. Russo, and G. Botter (2011), Catchment travel time distributions and water flow in soils, *Water Resources Research*, *47*, doi:10.1029/2011WR010478.

Stanford, J. A., and J. V. Ward (1993), An ecosystem perspective of alluvial rivers: Connectivity and the hyporheic corridor, *J. North Am. Benthol. Soc.*, *12*(1), 48–60.

Stonedahl, S. H., J. W. Harvey, A. Wörman, M. Salehin, and A. I. Packman (2010), A multiscale model for integrating hyporheic exchange from ripples to meanders, *Water Resour. Res.*, *46*, W12539, doi:10.1029/2009WR008865.

Tonina, D. (2012), Surface water and streambed sediment interaction: The hyporheic exchange, in *Fluid Mechanics of Environmental Interfaces*, chap. 9, edited by Carlo Gualtieri and Dragutin T. Mihailovic, pp. 255–294, CRC Press, Boca Raton, Fla.

Tonina, D., and A. Bellin (2008), Effects of pore-scale dispersion, degree of heterogeneity, sampling size, and source volume on the concentration moments of conservative solutes in heterogeneous formations, *Adv. Water Resour 31*(2), 339–354, doi:10.1016/j.advwatres.2007.08.009.

Tonina, D., and J. M. Buffington (2009a), A three-dimensional model for analyzing the effects of salmon redds on hyporheic exchange and egg pocket habitat, *Can. J. Fish. Aquat. Sci.*, *66*, 2157–2173.

Tonina, D., and J. M. Buffington (2009b), Hyporheic exchange in mountain rivers I: Mechanics and environmental effects, *Geogr. Compass*, *3*(3), 1063–1086.

Trauth, N., C. Schimdt, U. Maier, M. Vieweg, and J. H. Fleckenstein (2013), Coupled 3-D stream flow and hyporheic flow model under varying stream and ambient groundwater flow conditions in pool-riffle system, *Water Resour. Res.*, *49*, 5834–5850, doi:10.1002/wrcr.20442.

Zuber, A. (1986), On the interpretation of tracer data in variable flow systems, *J. Hydrol.*, *86*, 45–57.